

**PERSIANN-CCS-CDR, A 3-hourly 0.04° global precipitation
climate data record for heavy precipitation studies**

Mojtaba Sadeghi¹, Phu Nguyen¹, Matin Rahnamay Naeini¹, Kuolin Hsu¹, Dan Braithwaite¹,
Soroosh Sorooshian^{1,2}

1. Center for Hydrometeorology and Remote Sensing (CHRS), The Henry Samueli School
of Engineering, Department of Civil and Environmental Engineering, University of
California, Irvine, CA 92697, USA

2. Department of Earth System Science, University of California Irvine, 3200 Croul Hall,
Irvine, CA 92697-2175, USA

* Correspondence: mojtabas@uci.edu

Abstract

Accurate long-term global precipitation estimates, especially for heavy precipitation rates, at fine spatial and temporal resolutions is vital for a wide variety of climatological studies. Most of the available operational precipitation estimation datasets provide either high spatial resolution with short-term duration estimates or lower spatial resolution with long-term duration estimates. Furthermore, previous research has stressed that most of the available satellite-based precipitation products show poor performance for capturing extreme events at high temporal resolution. Therefore, there is a need for a precipitation product that reliably detects heavy precipitation rates with fine spatiotemporal resolution and a longer period of record. Precipitation Estimation from Remotely Sensed Information using Artificial Neural Networks-Cloud Classification System-Climate Data Record (PERSIANN-CCS-CDR) is designed to address these limitations. This dataset provides precipitation estimates at 0.04° spatial and 3-hourly temporal resolutions from 1983 to present over the global domain of 60°S to 60°N . Evaluations of PERSIANN-CCS-CDR and PERSIANN-CDR against gauge and radar observations show the better performance of PERSIANN-CCS-CDR in representing the spatiotemporal resolution, magnitude, and spatial distribution patterns of precipitation, especially for extreme events.

59 **Background & Summary**

60 Precipitation is widely recognized as the main driving component for the global
61 hydrological cycle and has an essential role for regulating the climate system ^{1,2}. Providing
62 reliable estimation of precipitation, especially heavy precipitation, at fine spatial and
63 temporal resolutions is crucial for many hydrological applications, including the
64 development of water resources management and planning strategies, the development of
65 early warning systems, as well as climatological studies. ³⁻⁷.

66 During the last three decades, a series of satellite-derived global precipitation datasets
67 have been developed and made operational (for an overview, see Maggioni et al., 2016; Sun
68 et al., 2018). Table 1 lists the spatiotemporal resolution and time coverage for the most widely
69 used operational satellite-based precipitation products. These datasets vary from 0.04 to 2.5
70 degrees in terms of spatial resolution, from 30 minutes to monthly in terms of temporal
71 resolution and up to 40 years of temporal span. These datasets have been designed for
72 different applications and their usability depends upon the type of application along with the
73 accuracy, latency, and temporal and spatial resolutions of the estimates.

74 Climate studies applications require long-term precipitation records ¹⁰; the World
75 Meteorological Organization (WMO) reported that at least 30 years of weather information
76 is needed for climatological studies ^{11,12}. Therefore, a reliable long-term global precipitation
77 estimation product is crucial for climatological studies. On the other hand, several studies
78 have shown that spatial-temporal variability of precipitation plays an important role in
79 catchment response and performance of hydrological models. Therefore, developing a
80 precipitation dataset with high spatial and temporal resolution is needed in order to represent
81 urban runoff processes well ¹³⁻¹⁸. For example, Lobligeois et al. ¹³ investigated the impact of
82 the spatial resolution of precipitation inputs on the performance of semi-distributed
83 hydrological models over 181 catchments with a variety of sizes and climate conditions. They
84 concluded that semi-distributed models significantly outperform lumped models when
85 precipitation inputs have higher spatial resolution, while they perform similarly when
86 precipitation have low spatial resolution. Huang et al. ¹⁵ explored the sensitivity of

hydrological model performance to the temporal resolution of precipitation inputs using lumped and distributed models. They showed that providing sub daily precipitation estimates rather than daily inputs can significantly improve the performance of the hydrologic model.

Nonetheless, most of the available operational precipitation products are either high resolution/short-duration estimates or low resolution with long-term estimates¹⁹; therefore, there is a need for providing precipitation products with both fine spatial and temporal resolution and a long period of record. Precipitation products with such attributes would provide the opportunity for researchers to study the spatial details and complete evolutions of extreme events including hurricanes and convective storms in the context of historical events²⁰⁻²². Most of the currently available satellite-based precipitation estimation products are not ideal for detecting extreme events at high altitude²³ as well as at high temporal resolutions (3-hourly).^{5,24-27}. For example, Mehran et al. (2014) evaluated the performance of Tropical Rainfall Measuring Mission (TRMM) Multisatellite Precipitation Analysis (TMPA), Precipitation Estimation from Remotely Sensed Information Using Artificial Neural Networks (PERSIANN) and CPC MORPHing technique (CMORPH) for detecting heavy precipitation rates against Stage IV radar observations over the CONUS. They showed that all these precipitation datasets miss a significant volume of rainfall. They concluded that none of the 3-hourly estimates from these products are suitable for detecting extreme events and their detection skills decrease dramatically as the extreme threshold increases. Precipitation Estimation from Remotely Sensed Information using Artificial Neural Networks-Cloud Classification System-Climate Data Record (PERSIANN-CCS-CDR), which provides 0.04° spatial and 3-hourly temporal resolution estimates from 1983 to present, has been explicitly designed to address the need for having a long term dataset with fine spatiotemporal resolution precipitation estimation which is reliable for extreme event detection.

Methods

Input data

Gridded satellite infrared data (GridSat-B1)

In 1983, the National Oceanic and Atmospheric Administration (NOAA)/National Climatic Data Center (NCDC) began collecting meteorological geostationary satellite data through the International Satellite Cloud Climatology Project (ISCCP)²⁸. The ISCCP B1 dataset provides global IR brightness temperature data with 10-km spatial and 3-hourly temporal resolution for the period from 1979 to present. The ISCCP B1 dataset consists of observations from different sensors launched by different countries, including United States [for the Geostationary Operational Environmental Satellite (GOES) series], Japan [for the Japanese Geostationary Meteorological Satellite (GMS) series and Multi-functional Transport Satellite (MTSAT)], Europe [for the European Meteorological satellite (Meteosat) series], and China [for the Chinese Fen-Yung 2 (FY2) series]. The gridded satellite (GridSat-B1) dataset is derived from the ISCCP B1 dataset and provides near-global data with 0.07° spatial and 3-hourly temporal resolution from 1980 to present. The GridSat-B1 dataset is available via (<https://www.ncdc.noaa.gov/gridsat/gridsat-index.php>). More information can be found in Knapp et al.²⁹.

NOAA Climate Prediction Center (CPC-4km) IR product

The NOAA Climate Prediction Center (CPC) globally merged IR product, which is referred to as CPC-4km, was developed to provide near-real time data for monitoring global precipitation³⁰. This dataset offers near-global (60°N-60°S) IR data with 4-km spatial and half-hourly temporal resolutions from the present international constellation of operational geostationary meteorological satellites for the period from 2000 to present. The CPC-4km product is comprised of IR observations from several international GEO satellites, including Meteosat-5 and Meteosat-7, GMS, and GOES. CPC-4km data is publicly accessible through the Climate Prediction Center webpage (https://www.cpc.ncep.noaa.gov/products/global_precip/html/web.shtml)

Global Precipitation Climatology Project (GPCP V2.3)

GPCP is part of the Global Energy and Water Cycle Exchanges (GEWEX) project under the World Climate Research Program (WCRP)³¹. This product provides monthly precipitation at a 2.5° x 2.5° spatial resolution by merging different satellite-based estimation information (passive microwave/infrared) along with precipitation gauge networks from GPCC. A comprehensive description of GPCP monthly v2.3 data inputs and the merging process can be found in³². The GPCP dataset is available for public use through the Earth System Science Interdisciplinary Center (ESSIC) and Cooperative Institute for Climate and Satellites (CICS), University of Maryland College Park (<http://gpcp.umd.edu>).

Reference Data

CPC Global Unified Gauge-Based Analysis of Daily Precipitation

The National Oceanic and Atmospheric Administration (NOAA) Climate Prediction Center (CPC) provides the CPC Global Unified Gauge-Based Analysis of Daily Precipitation dataset³³. This dataset offers global precipitation estimates at 0.5° x 0.5° spatial and daily temporal resolutions from 1979 to present. The daily precipitation reports of roughly 30,000 stations from different sources across global land areas have been collected and quality controlled by the NOAA Climate Prediction Center. The data sources include Global Telecommunication System (GTS), the CPC unified daily gauge datasets over the CONUS, Cooperative Observer Network (COOP), and other national and international agencies. A comprehensive description of this CPC dataset and the interpolation algorithm that is used can be found in Xie et al.³⁴. The CPC Global Unified Gauge-Based Analysis of Daily Precipitation dataset is accessible to the public through (<ftp://ftp.cdc.noaa.gov/Datasets>).

NCEP Stage IV QPE Data

NCEP Stage IV QPE is widely considered as the best long-term gridded rain accumulation dataset over the CONUS due to its extensive quality control procedures^{5,35}. This product merges the national Weather Surveillance Radar-1988 Doppler (WSR-88D) network of ground radars and ground-based rain gauge observations^{36,37}. NCEP Stage IV

170 provides precipitation observations at 0.04° (4 km) spatial resolution and hourly, 6 hourly,
171 and 24 hourly temporal resolution. For this study, daily NCEP Stage IV observations were
172 obtained from the distribution
173 website (<http://www.emc.ncep.noaa.gov/mmb/ylin/pcpanl/stage4/>) and used as the
174 benchmark for evaluating the remotely sensed precipitation datasets over the CONUS.

175 **Precipitation Estimation from Remotely Sensed Information using** 176 **Artificial Neural Networks–Climate Data Record (PERSIANN-CDR)**

177 PERSIANN-CDR is a satellite-based precipitation estimation product that provides more
178 than three decades (from 1983 to present) of daily precipitation estimates at $0.25^\circ \times 0.25^\circ$
179 spatial resolution for the 60°S–60°N latitude band ¹². PERSIANN-CDR utilizes the archive
180 of infrared brightness temperature from GridSat-B1 ^{28,38} as the input of the PERSIANN
181 algorithm. Then the rainfall estimates of the PERSIANN algorithm are bias corrected using
182 the monthly Global Precipitation Climatology Project (GPCP) version 2.3 product at $2.5^\circ \times$
183 2.5° spatial resolution ³⁹. This dataset is available for public access through the NOAA
184 National Centers for Environmental Information (NCEI) Program
185 (<https://www.ncdc.noaa.gov/cdr>) and through the Center for Hydrometeorology and Remote
186 Sensing (CHRS) Data Portal (<http://chrsdata.eng.uci.edu/>). Additional details about the
187 PERSIANN-CDR algorithm can be found in Ashouri et al. ¹² and Sadeghi et al. ^{39,40}.

188

189 **PERSIANN-CCS-CDR Methodology description**

190 PERSIANN-CCS-CDR is generated beginning with rain rate (RR) outputs from the
191 PERSIANN-CCS model. It should be noted that the PERSIANN-CCS algorithm utilizes one
192 global IR image to estimate the rainfall for that corresponding time step. The IR inputs used
193 by PERSIANN-CCS to generate RR outputs come from two distinct periods: From 1983
194 through February 2000 GridSat-B1 IR data are used but from March 2000 to the present
195 CPC-4km IR data are available and those are used instead. All IR inputs are resampled to
196 0.04° resolution before input. The GridSat-B1 images are every 3 hours and the output RR

data are mm/hr rain rates every 3 hours. The input CPC-4km images are available every 30-minutes, so the output RR data are mm/hr rain rates every 30-minutes.

In the second stage of the PERSIANN-CCS-CDR model the 0.04° RR grids, after a threshold (thd) of 0.1 mm/3hr is applied, are aggregated to monthly temporal resolution for comparison to monthly GPCP v2.3 precipitation. Due to the nature of satellite IR data, some fractions of non-raining pixels are falsely associated with light precipitation in the PERSIANN-CCS-CDR algorithm. We applied a threshold (thd) of 0.1 mm/hr to eliminate these falsely assigned light rain rate values. The monthly PERSIANN-CCS RR accumulations (mm/month) at 0.04° spatial resolution must be aggregated then to 2.5° using the bilinear method to match GPCP v2.3.

$$R_{\text{Cum-PERSIANN-CCS}}(i', j') = \sum^{nd} \sum^{nh} (\sum^{62} \sum^{62} [r_{\text{PERSIANN-CCS}}(i, j) \geq \text{thd}]) \quad (\text{Eq.1})$$

In this equation, $R_{\text{Cum-PERSIANN-CCS}}$ and $r_{\text{PERSIANN-CCS}}$ are the monthly 2.5° aggregated PERSIANN-CCS estimates and 30min/3-hourly PERSIANN-CCS estimates at 0.04° spatial resolution, respectively. The i and j represent the latitude and longitude of the 30min/3-hourly PERSIANN-CCS at 0.04° × 0.04° spatial resolution. Similarly, i' and j' are the latitude and longitude of the aggregated PERSIANN-CCS at 2.5° × 2.5° resolution. The nd and nh are the number of days and the number of 30min/3-hourly PERSIANN-CCS samples in each day, respectively.

In the next stage, the bias-adjustment weights for each monthly 2.5° grid cell are calculated as follows:

$$w(i', j') = R_{\text{GPCP}}(i', j') / R_{\text{Cum-PERSIANN-CCS}}(i', j'), \quad 0 \leq w \leq 2.5, \quad (\text{Eq.2})$$

where R_{GPCP} is the monthly rain rate of GPCP for a given pixel.

The 2.5° weights grids must then be bilinearly interpolated back to 0.04° spatial resolution for the next stage. Our experiments showed that some locations with very low monthly rainfall values, such as high latitudes and very dry regions, the weight (w) can become large. This can lead to unreasonably large 3-hourly rainfalls at finer resolution. To prevent such cases, we applied a maximum weight of 2.5. In the final 2 stages, the 0.04° monthly weights

are applied to each original input RR grid available. Each RR grid, either every 3 hours RR or every 30-minute RR depending on the IR data source, is multiplied by the weight.

$$\text{PERSIANN} - \text{CCS} - \text{CDR}(i, j) = w(i, j) * r_{\text{PERSIANN-CCS}}(i, j) \quad (\text{Eq. 3})$$

Finally, the bias-adjusted RR files are aggregated to produce the final PERSIANN-CCS-CDR product, consisting of an accumulation at 3-hourly resolution and 0.04° spatial resolution. Due to the limitation of IR information and precipitation algorithm, the RR mm/hr are limited by a historical maximum rain rate for each local region and each calendar month for seasonal and geographical specificity. We monitor this threshold over the time, and we will adjust this threshold to consider the climate change.

~~At this last stage the RR mm/hr are limited by a historical maximum rain rate for each local region and each calendar month for seasonal and geographical specificity.~~

235

Data Records

A near-global 37+ year high-resolution precipitation dataset with high spatial and temporal

resolution is now available. PERSIANN-CCS-CDR developed by the Center for Hydrometeorology and Remote Sensing (CHRS) at the University of California, Irvine (UCI) provides precipitation estimates at 0.04° spatial and 3-hourly temporal resolutions from 1983 to present over the global domain of 60°S to 60°N. PERSIANN-CCS-CDR data are publicly available through CHRS Data Portal (<https://chrsdata.eng.uci.edu/>) and also on our FTP site (<ftp://persiann.eng.uci.edu/CHRSdata/PCCSCDR/>) for a number of time steps (3-hourly, 6-hourly, and daily), and different formats (NetCDF, GeoTiff, and Esri BIL) from 1983 to present. The detailed description of the data format can be found in the provided FTP link⁴¹.

247

Formatted: Line spacing: 1.5 lines

Technical Validation

Performance Evaluation for extreme events over the Globe and the CONUS

Figure 1 presents the performance of PERSIANN-CDR and PERSIANN-CCS-CDR against CPC in detecting the 99th percentile indices (RR99p) of the daily precipitation on wet days (days with daily precipitation ≥ 1 mm) for the period of 1983 to 2019 over global land areas. The CPC unified gauge-based analysis dataset at $0.5^\circ \times 0.5^\circ$ spatial resolution is used as a gauge-based reference for comparing and calculating the continuous evaluation indices including CC, RMSE, and MSE. The original 0.25° PERSIANN-CDR and 0.04° PERSIANN-CCS-CDR datasets are resampled to 0.5° spatial resolution using the bilinear interpolation method to match the spatial resolution of the CPC dataset. Then, the 99th percentile of daily precipitation of CPC, PERSIANN-CDR, and PERSIANN-CCS-CDR datasets were calculated for each pixel using the whole period of record (1983-2019). Clearly in Figure 1, PERSIANN-CCS-CDR offers more accuracy for the intensity of rain rates in comparison to PERSIANN-CDR in terms of estimating extreme events. PERSIANN-CDR tends to underestimate heavy precipitation over the globe, while PERSIANN-CCS-CDR provides a more realistic representation of heavy precipitation. Figure 1 also reveals that PERSIANN-CCS-CDR's estimates have both higher correlation and lower RMSE with CPC observations compared to PERSIANN-CDR over the globe. The correlation between PERSIANN-CCS-CDR and CPC unified gauge-based analysis over land is increased by 15%, and the RMSE decreased by 28%, respectively, versus PERSIANN-CDR.

Figure 2 shows the performance of PERSIANN-CDR and PERSIANN-CCS-CDR against Stage IV, as a reference, in capturing the RR99p of daily precipitation at $0.25^\circ \times 0.25^\circ$ spatial resolution for the period of 2003 to 2019. We used daily Stage IV images, which depict 24-hour total precipitation ending at 1200 UTC. In addition, we utilized the PERSIANN-CDR and PERSIANN-CCS-CDR estimates with the same end of day definition. The PERSIANN-CCS-CDR estimates were resampled to 0.25° spatial and daily temporal resolution using the bilinear method for the comparison. As shown in Figure 2, high values of RR99p appear in the southeastern part of the United States. In general, PERSIANN-CCS-CDR captures the

magnitude and the pattern of RR99p better than PERSIANN-CDR compared to radar observations, especially over the southeastern part of the CONUS. Although PERSIANN-CDR shows similar patterns to Stage IV, it underestimates magnitudes of precipitation. On the other hand, PERSIANN-CCS-CDR captures the volume of the extreme events fairly well. The disagreement between PERSIANN-CCS-CDR and Stage IV radar observations is mainly over the northern part of the United States, including Minnesota, Iowa, and Michigan, where most values are overestimated. According to Figure 2, the spatial correlation, RMSE, and MSE of PERSIANN-CDR and PERSIANN-CCS-CDR with respect to CPC unified gauge-based analysis indicate that PERSIANN-CCS-CDR has better performance than PERSIANN-CDR for extreme event analyses in climatological applications. CC and RMSE of PERSIANN-CCS-CDR estimates with Stage IV are improved by 25% and 31%, in comparison to PERSIANN-CDR, respectively. PERSIANN-CCS is an improvement of the PERSIANN algorithm; Instead of direct pixel-to-pixel fitting of IR cloud top temperature to the rain rate, PERSIANN-CCS leverages objective classification methods in order to classify each IR image into a number of cloud patch groups based on feature similarity including patch size and texture. This feature results in higher performance of PERSIANN-CCS compared to PERSIANN in capturing extreme precipitation. Utilizing PERSIANN-CCS estimates as inputs to PERSIANN-CCS-CDR leads to improved performance in capturing extreme precipitation compared to PERSIANN-CDR, which uses PERSIANN estimates.

Case Studies

To further investigate the performance of PERSIANN-CCS-CDR estimates with Stage IV as a reference, the following verification studies have been done at different temporal and spatial resolutions. The first case study targets Hurricane Harvey in 2017 and investigates the performance of the PERSIANN-CCS-CDR estimates over the Southeastern United States at daily temporal resolution. The second case study is related to the flood that occurred in Louisiana in 2016 and evaluates the performance of the developed product at the watershed scale for 3-hourly and daily temporal scales.

Hurricane Harvey, August 2017 (Daily Assessment)

During August 25-30, 2017, Hurricane Harvey hit the Southeastern regions of the United States, including Southeast Texas, and Louisiana. Hurricane Harvey is classified as a Category 4 storm that caused catastrophic damages. This storm is referred as one of the costliest extreme precipitation events that struck in the history of the United States⁴². According to the National Hurricane Center, the total damage is estimated to be more than \$125 billion and it is confirmed that there were more than 80 fatalities⁴³. In this section, PERSIANN-CCS-CDR and PERSIANN-CDR are evaluated against Stage IV as the reference at 0.25° spatial resolution and daily temporal resolution. The original 0.04° × 0.04° spatial resolution of Stage IV and PERSIANN-CCS-CDR datasets were resampled to 0.25° × 0.25° spatial resolution using bilinear interpolation to match the spatial resolution of PERSIANN-CDR. Then the 3-hourly estimates of PERSIANN-CCS-CDR were aggregated to obtain daily scale to match the PERSIANN-CDR estimates in temporal resolution. Figure 3 presents daily values for extreme precipitation that occurred from August 27 to 30, 2017 using Stage IV data and PERSIANN-CDR and PERSIANN-CCS-CDR estimates. As shown in Figure 3, PERSIANN-CCS-CDR captures both the spatial pattern and the intensity of rainfall better than PERSIANN-CDR. For more exploration of the accuracy of estimation, the scatter plots for PERSIANN-CDR and PERSIANN-CCS-CDR versus Stage IV are presented and the relevant statistics are calculated in Figure 3. In general, PERSIANN-CCS-CDR outperforms PERSIANN-CDR for CC and FAR. As shown in Figure 3, both PERSIANN-CDR and PERSIANN-CCS-CDR show a high correlation with Stage IV radar. The correlation for PERSIANN-CDR and PERSIANN-CCS-CDR with Stage IV are 0.79 and 0.84, respectively. RMSE improves from 20 mm/day to 18.7 mm/day for PERSIANN-CCS-CDR estimates compared to PERSIANN-CDR. Furthermore, PERSIANN-CDR underestimates intense precipitation, while PERSIANN-CCS-CDR performs relatively well. As can be seen, both Stage IV and PERSIANN-CCS-CDR show rain rates with more than 500 mm/day that occurred over some pixels. However, PERSIANN-CDR does not show any value more than 195 mm/day and underestimates the rain rates.

Louisiana Flood, August 12, 2016 (3-hourly, and Daily Assessment)

In August 2016, an intense rainfall event occurred over the state of Louisiana with more than 30 inches (760 millimeters) of rainfall in some locations, resulting in a catastrophic flood (<https://www.usgs.gov/news/>). This event led to more than a dozen deaths and more than \$30 million in damages (<https://www.cnn.com/>). The performances of PERSIANN-CDR and PERSIANN-CCS-CDR for this flood are evaluated against Stage IV radar observations (Figure 4). Figure 4b shows Stage IV rainfall estimates at $0.04^\circ \times 0.04^\circ$ spatial resolution on August 12, 2016. Figure 4c and figure 4d shows PERSIANN-CDR estimates (with a $0.25^\circ \times 0.25^\circ$ spatial resolution) and PERSIANN-CCS-CDR estimates (with a $0.04^\circ \times 0.04^\circ$ spatial resolution), respectively. This figure demonstrates two attractive aspects of the PERSIANN-CCS-CDR dataset in comparison to the PERSIANN-CDR dataset for climatological studies: 1) PERSIANN-CCS-CDR performs better than PERSIANN-CDR for this extreme event by capturing the volume of heavy rain over the southwest area of the watershed as shown. 2) The high temporal resolution of PERSIANN-CCS-CDR is another feature which is beneficial for studying the diurnal cycle and is essential for rainfall-runoff modeling studies. These two features of PERSIANN-CCS-CDR make this new dataset attractive for integrating its high spatiotemporal resolution estimates into hydrological and land-surface models for flood forecasting (or other applications that are sensitive to heavy precipitation rates).

Figure 5 illustrates the evolution of the precipitation that occurred on August 12, 2016 based on Stage IV and PERSIANN-CCS-CDR estimates at 3-hourly temporal and $0.04^\circ \times 0.04^\circ$ spatial resolutions. The hourly estimates of Stage IV data are aggregated to a 3-hourly scale to match the PERSIANN-CCS-CDR data in temporal resolution. This figure demonstrates the superior performance of PERSIANN-CCS-CDR in detecting the magnitude of precipitation at the 3-hourly temporal scale. For the period between 6:00 to 9:00 UTC, PERSIANN-CCS-CDR estimates the rain rates fairly well compared to Stage IV radar data; however, a southward shifting can be seen in PERSIANN-CCS-CDR's estimates. During 9:00 to 12:00 UTC, 12:00 to 15:00 and 15:00 to 18:00 UTC, PERSIANN-CCS-CDR successfully detects the amount of intense precipitation over the eastern regions of the watershed, yet it misses some parts of the rainfall that occurred over the central parts of the region. During 18:00 to 21:00 UTC, the PERSIANN-CCS-CDR detects most of the intense rainfall. A northward shift can be seen in PERSIANN-CCS-CDR's estimates for the period of 21:00 to 24:00 UTC. Table 2 summarizes PERSIANN-CCS-CDR performance in

detecting (POD, FAR, CSI) and estimating (RMSE, MAE, Correlation) rainfall intensity at 3-hourly temporal and $0.04^\circ \times 0.04^\circ$ spatial resolutions over the shown watershed on August 12, 2016. Figure 6 shows the 3-hourly estimates of Stage IV (blue) and PERSIANN-CCS-CDR (red) over the Louisiana watershed shown in figure 5 for the month of August 2016. It can be seen that PERSIANN-CCS-CDR can capture both the pattern and the 3-hourly peak precipitation relatively well compared to Stage IV as the reference. Specifically, the CC and RMSE of PERSIANN-CCS-CDR with Stage IV are 0.79 and 0.87 mm/3hr, respectively.

One of the most attractive features of PERSIANN-CCS-CDR is its improved performance for detecting heavy precipitation. While current operational satellite-based precipitation datasets provide significant opportunities for providing precipitation estimates at high spatiotemporal resolution over the globe, numerous studies have argued that most of them have a weakness in detecting heavy precipitation that occurs at high temporal resolution (sub-daily or 3-hourly).^{5,24} The current limitations for accurate estimation of extreme precipitation hinder the use of satellite-based precipitation datasets for applications that are sensitive to heavy rain rates such as designing warning systems, integrating precipitation data into hydrological models, etc. The performance of PERSIANN-CCS-CDR for heavy precipitation detection suggests that this dataset is an attractive dataset for the mentioned hydrological applications.

Another important feature of the PERSIANN-CCS-CDR dataset is the combination of high spatial and temporal resolution with a long period of record. A reliable long-term precipitation record with fine spatiotemporal resolution is essential for many applications including hydrological modelling, rainfall frequency analysis, and development of depth duration curves. However, the majority of current operational datasets are either high resolution with short-duration estimates or lower resolution with long-term estimates¹⁹. PERSIANN-CCS-CDR, which provides accurate estimations of extreme precipitation with fine spatiotemporal resolution ($0.04^\circ \times 0.04^\circ$ spatial and 3-hourly temporal resolution) from 1983 to present over the global domain of 60°S to 60°N , has been developed to address the lack of available datasets that meet both needs.

One of the few potential shortcomings of the PERSIANN-CCS-CDR dataset is that the available time scale of GridSat-B1 is 3-hourly, rather than hourly, for the period before 2000. This limits the capability of the dataset to that coarser temporal resolution for the period from 1983 to 2000. Another limitation is the PERSIANN-CCS algorithm's capability to capture the spatial patterns of rainfall. PERSIANN-CCS extracts cloud information based on manually defined features including coldness, texture, and geometry, which can limit its ability to accurately estimate rainfall because manual feature extraction is always biased toward the most relevant and physically obvious features that have direct impacts on precipitation occurrence. Due to the complexity of the precipitation phenomena, there may be some other factors as yet hidden to CHRS researchers that play crucial roles in the accuracy of the model's simulations. CHRS researchers are currently working on the development of even more advanced satellite retrieval algorithms by applying new data-driven methodologies to automatically extract features from the input datasets. While more research needs to be done to verify the performance of the developed dataset, this paper presents promising validation results and demonstrates example applications for the PERSIANN-CCS-CDR dataset. This newly introduced dataset provides an opportunity for scientists and stakeholders to leverage the more accurate estimates of PERSIANN-CCS-CDR to improve disaster mitigation models and strategies.

Code Availability

While the PERSIANN-CCS-CDR codes are not written as a portable library or toolset, access to the code is not restricted, and it is available upon users' requests.

Acknowledgements

The financial support of this research is from the U.S. Department of Energy (DOE Prime Award DE-IA0000018), the California Energy Commission (CEC Award 300-15-005), University of California (4600010378 TO15 Am 22), MASEEH fellowship, NOAA/NESDIS/NCDC (Prime Award NA09NES4400006 and NCSU CICS and Subaward 2009-1380-01). Also, support from the office of vice-chancellor for research of graduate students is acknowledged.

420

421 **Author contributions**

422 Conceptualization, M.S., P.N., K.H., and S.S.; methodology, M.S., P.N., D.B.; software,
423 M.S. and D.B.; validation, M.S., P.N., M.R.N.; formal analysis, M.S.; investigation, M.S. and
424 P.N.; resources, M.S., P.N., M.R.N.; data curation, M.S.; writing—original draft preparation,
425 M.S.; visualization, M.S.; supervision, S.S., K.H., and P.N.; project administration, M.S.;
426 funding acquisition, S.S.

427

428 **Competing interests**

429 The authors declare no competing interests.

430 **References**

- 431 1. Trenberth, K. E., Dai, A., Rasmussen, R. M. & Parsons, D. B. The changing character of
432 precipitation. *Bull. Am. Meteorol. Soc.* **84**, 1205–1218 (2003).
- 433 2. Wang, B., Liu, J., Kim, H.-J., Webster, P. J. & Yim, S.-Y. Recent change of the global
434 monsoon precipitation (1979–2008). *Clim. Dyn.* **39**, 1123–1135 (2012).
- 435 3. Hou, A. Y. *et al.* The global precipitation measurement mission. *Bull. Am. Meteorol. Soc.* **95**,
436 701–722 (2014).
- 437 4. Nguyen, P. *et al.* Global precipitation trends across spatial scales using satellite observations.
438 *Bull. Am. Meteorol. Soc.* **99**, 689–697 (2018).
- 439 5. Mehran, A. & AghaKouchak, A. Capabilities of satellite precipitation datasets to estimate
440 heavy precipitation rates at different temporal accumulations. *Hydrol. Process.* **28**, 2262–2270
441 (2014).
- 442 6. Nguyen, P., Thorstensen, A., Sorooshian, S., Hsu, K. & AghaKouchak, A. Flood forecasting
443 and inundation mapping using HiResFlood-UCI and near-real-time satellite precipitation data:
444 The 2008 Iowa flood. *J. Hydrometeorol.* **16**, 1171–1183 (2015).
- 445 7. Sadeghi, M. *et al.* PERSIANN-CNN: Precipitation Estimation from Remotely Sensed
446 Information Using Artificial Neural Networks–Convolutional Neural Networks. *J.*
447 *Hydrometeorol.* **20**, 2273–2289 (2019).

- 448 8. Maggioni, V., Meyers, P. C. & Robinson, M. D. A review of merged high-resolution satellite
449 precipitation product accuracy during the Tropical Rainfall Measuring Mission (TRMM) era.
450 *J. Hydrometeorol.* **17**, 1101–1117 (2016).
- 451 9. Sun, Q. *et al.* A review of global precipitation data sets: Data sources, estimation, and
452 intercomparisons. *Rev. Geophys.* **56**, 79–107 (2018).
- 453 10. Wentz, F. J., Ricciardulli, L., Hilburn, K. & Mears, C. How much more rain will global
454 warming bring? *Science (80-.)*. **317**, 233–235 (2007).
- 455 11. Burroughs, W. & Burroughs, W. S. *Climate: Into the 21st century*. (Cambridge University
456 Press, 2003).
- 457 12. Ashouri, H. *et al.* PERSIANN-CDR: Daily precipitation climate data record from
458 multisatellite observations for hydrological and climate studies. *Bull. Am. Meteorol. Soc.* **96**,
459 69–83 (2015).
- 460 13. Lobligeois, F., Andréassian, V., Perrin, C., Tabary, P. & Loumagne, C. When does higher
461 spatial resolution rainfall information improve streamflow simulation? An evaluation using
462 3620 flood events. (2014).
- 463 14. Vieux, B. E. & Imgarten, J. M. On the scale-dependent propagation of hydrologic uncertainty
464 using high-resolution X-band radar rainfall estimates. *Atmos. Res.* **103**, 96–105 (2012).
- 465 15. Huang, Y., Bárdossy, A. & Zhang, K. Sensitivity of hydrological models to temporal and
466 spatial resolutions of rainfall data. *Hydrol. Earth Syst. Sci.* **23**, 2647–2663 (2019).
- 467 16. Cristiano, E., ten Veldhuis, M. & van de Giesen, N. Spatial and temporal variability of rainfall
468 and their effects on hydrological response in urban areas-a review. *Hydrol. Earth Syst. Sci.* **21**,
469 (2017).
- 470 17. Ficchi, A., Perrin, C. & Andréassian, V. Impact of temporal resolution of inputs on
471 hydrological model performance: An analysis based on 2400 flood events. *J. Hydrol.* **538**,
472 454–470 (2016).
- 473 18. Lee, M., Im, E. & Bae, D. Impact of the spatial variability of daily precipitation on
474 hydrological projections: A comparison of GCM-and RCM-driven cases in the Han River
475 basin, Korea. *Hydrol. Process.* **33**, 2240–2257 (2019).

- 476 19. Kidd, C. & Levizzani, V. Status of satellite precipitation retrievals. *Hydrol. Earth Syst. Sci.*
477 **15**, 1109–1116 (2011).
- 478 20. Funk, C. *et al.* The climate hazards infrared precipitation with stations—a new environmental
479 record for monitoring extremes. *Sci. data* **2**, 1–21 (2015).
- 480 21. Yoshimoto, S. & Amarnath, G. Applications of satellite-based rainfall estimates in flood
481 inundation modeling—A case study in Mundeni Aru River Basin, Sri Lanka. *Remote Sens.* **9**,
482 998 (2017).
- 483 22. Sadeghi, M. *et al.* Precipitation Estimation from Remotely Sensed Information using Artificial
484 Neural Networks-Cloud Classification System-Climate Data Record (PERSIANN-CCS-
485 CDR). *AGU FM* **2019**, H13P-1964 (2019).
- 486 23. Libertino, A., Sharma, A., Lakshmi, V. & Claps, P. A global assessment of the timing of
487 extreme rainfall from TRMM and GPM for improving hydrologic design. *Environ. Res. Lett.*
488 **11**, 54003 (2016).
- 489 24. AghaKouchak, A., Behrangi, A., Sorooshian, S., Hsu, K. & Amitai, E. Evaluation of satellite-
490 retrieved extreme precipitation rates across the central United States. *J. Geophys. Res. Atmos.*
491 **116**, (2011).
- 492 25. Anagnostou, E. N. *et al.* Benchmarking high-resolution global satellite rainfall products to
493 radar and rain-gauge rainfall estimates. *IEEE Trans. Geosci. Remote Sens.* **48**, 1667–1683
494 (2009).
- 495 26. Liu, C. & Zipser, E. J. The global distribution of largest, deepest, and most intense
496 precipitation systems. *Geophys. Res. Lett.* **42**, 3591–3595 (2015).
- 497 27. Prakash, S., Sathiyamoorthy, V., Mahesh, C. & Gairola, R. M. An evaluation of high-
498 resolution multisatellite rainfall products over the Indian monsoon region. *Int. J. Remote Sens.*
499 **35**, 3018–3035 (2014).
- 500 28. Knapp, K. R. Scientific data stewardship of International Satellite Cloud Climatology Project
501 B1 global geostationary observations. *J. Appl. Remote Sens.* **2**, 23548 (2008).
- 502 29. Knapp, K. R. *et al.* Globally gridded satellite observations for climate studies. *Bull. Am.*
503 *Meteorol. Soc.* **92**, 893–907 (2011).

- 504 30. Janowiak, J. E., Joyce, R. J. & Yarosh, Y. A real-time global half-hourly pixel-resolution
505 infrared dataset and its applications. *Bull. Am. Meteorol. Soc.* **82**, 205–218 (2001).
- 506 31. Huffman, G. J. *et al.* The global precipitation climatology project (GPCP) combined
507 precipitation dataset. *Bull. Am. Meteorol. Soc.* **78**, 5–20 (1997).
- 508 32. Adler, R. F. *et al.* The Global Precipitation Climatology Project (GPCP) monthly analysis
509 (new version 2.3) and a review of 2017 global precipitation. *Atmosphere (Basel)*. **9**, 138
510 (2018).
- 511 33. Chen, M. *et al.* Assessing objective techniques for gauge-based analyses of global daily
512 precipitation. *J. Geophys. Res. Atmos.* **113**, (2008).
- 513 34. Xie, P. *et al.* A gauge-based analysis of daily precipitation over East Asia. *J. Hydrometeorol.*
514 **8**, 607–626 (2007).
- 515 35. Smalley, M., L’Ecuyer, T., Lebsock, M. & Haynes, J. A comparison of precipitation
516 occurrence from the NCEP Stage IV QPE product and the CloudSat Cloud Profiling Radar. *J.*
517 *Hydrometeorol.* **15**, 444–458 (2014).
- 518 36. Lin, Y. & Mitchell, K. E. 1.2 the NCEP stage II/IV hourly precipitation analyses: Development
519 and applications. in *19th Conf. Hydrology, American Meteorological Society, San Diego, CA,*
520 *USA* (Citeseer, 2005).
- 521 37. Wu, W., Kitzmiller, D. & Wu, S. Evaluation of radar precipitation estimates from the National
522 Mosaic and Multisensor Quantitative Precipitation Estimation System and the WSR-88D
523 precipitation processing system over the conterminous United States. *J. Hydrometeorol.* **13**,
524 1080–1093 (2012).
- 525 38. Rossow, W. B. & Duenas, E. N. The international satellite cloud climatology project (ISCCP)
526 web site: An online resource for research. *Bull. Am. Meteorol. Soc.* **85**, 167–172 (2004).
- 527 39. Sadeghi, M. *et al.* Evaluation of PERSIANN-CDR Constructed Using GPCP V2. 2 and V2. 3
528 and A Comparison with TRMM 3B42 V7 and CPC Unified Gauge-Based Analysis in Global
529 Scale. *Remote Sens.* **11**, 2755 (2019).
- 530 40. Sadeghi, M. Assessment of the PERSIANN-CDR Products Bias-corrected with the GPCP
531 Datasets Versions 2.2 & 2.3. (2018).

532 41. Sorooshian, S. PERSIANN-CCS-CDR. CHRS UC Irvine
533 <https://doi.org/10.11572/P24W2F> (2020).

534 42. Amadeo, K. Hurricane Harvey facts, damage and costs. *Balanc. Retrieved from https://www.*
535 *thebalance.com/hurricane-harvey-facts-damage-costs-4150087* (2018).

536 43. Van Oldenborgh, G. J. *et al.* Attribution of extreme rainfall from Hurricane Harvey, August
537 2017. *Environ. Res. Lett.* **12**, 124009 (2017).

538 44. Xie, P. & Arkin, P. A. Global precipitation: A 17-year monthly analysis based on gauge
539 observations, satellite estimates, and numerical model outputs. *Bull. Am. Meteorol. Soc.* **78**,
540 2539–2558 (1997).

541 45. Joyce, R. J., Janowiak, J. E., Arkin, P. A. & Xie, P. CMORPH: A method that produces global
542 precipitation estimates from passive microwave and infrared data at high spatial and temporal
543 resolution. *J. Hydrometeorol.* **5**, 487–503 (2004).

544 46. Huffman, G. J. *et al.* Global precipitation at one-degree daily resolution from multisatellite
545 observations. *J. Hydrometeorol.* **2**, 36–50 (2001).

546 47. Huffman, G. J. *et al.* NASA global precipitation measurement (GPM) integrated multi-satellite
547 retrievals for GPM (IMERG). *Algorithm Theor. Basis Doc. Version 4*, 26 (2015).

548 48. Beck, H. E. *et al.* MSWEP: 3-hourly 0.25 global gridded precipitation (1979–2015) by
549 merging gauge, satellite, and reanalysis data. *Hydrol. Earth Syst. Sci.* **21**, 589–615 (2017).

550 49. Beck, H. E. *et al.* Daily evaluation of 26 precipitation datasets using Stage-IV gauge-radar
551 data for the CONUS. *Hydrol. Earth Syst. Sci.* **23**, (2019).

552 50. Hsu, K., Gao, X., Sorooshian, S. & Gupta, H. V. Precipitation estimation from remotely sensed
553 information using artificial neural networks. *J. Appl. Meteorol.* **36**, 1176–1190 (1997).

554 51. Hong, Y., Gochis, D., Cheng, J., Hsu, K. & Sorooshian, S. Evaluation of PERSIANN-CCS
555 rainfall measurement using the NAME event rain gauge network. *J. Hydrometeorol.* **8**, 469–
556 482 (2007).

557 52. Huffman, G. J. *et al.* The TRMM multisatellite precipitation analysis (TMPA): Quasi-global,
558 multiyear, combined-sensor precipitation estimates at fine scales. *J. Hydrometeorol.* **8**, 38–55
559 (2007).

Table of Figures

Figure 1 Evaluation of PERSIANN-CDR and PERSIANN-CCS-CDR against CPC for the 99th percentile of daily precipitation on wet days (days with daily precipitation ≥ 1 mm) for the period of 1983-2019.

Figure 2 Evaluation of PERSIANN-CDR and PERSIANN-CCS-CDR against Stage IV for the 99th percentile of daily precipitation on wet days (days with daily precipitation ≥ 1 mm) for the period of 2003-2019.

Figure 3 The spatial precipitation evolution of Hurricane Harvey for the period from August 26-30, 2017 from (a) Stage IV, (b) PERSIANN-CDR, and (c) PERSIANN-CCS-CDR

Figure 4 Evaluation of daily PERSIANN-CDR and PERSIANN-CCS-CDR against Stage IV for the Louisiana flood of Aug. 12, 2016.

590 Figure 5 Evaluation of 3-hourly PERSIANN-CCS-CDR against Stage IV for the Louisiana
591 flood of Aug. 12, 2016.

594 Figure 6 3-hourly estimates of Stage IV and PERSIANN-CCS-CDR over the Louisiana
595 watershed shown in figure 5 for the month of August, 2016.

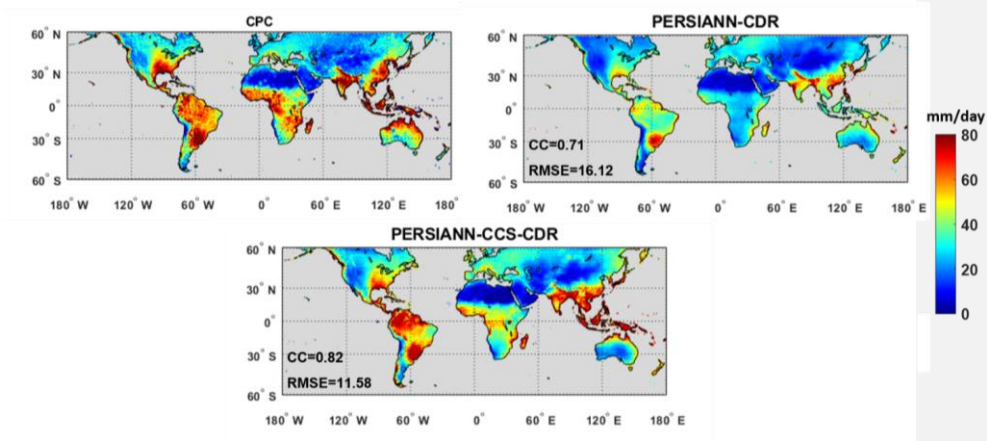
596
597
598
599

600 **Figures**

601
602
603

604 **Figure 1**

605
606
607
608
609
610



611
612
613

Figure 2

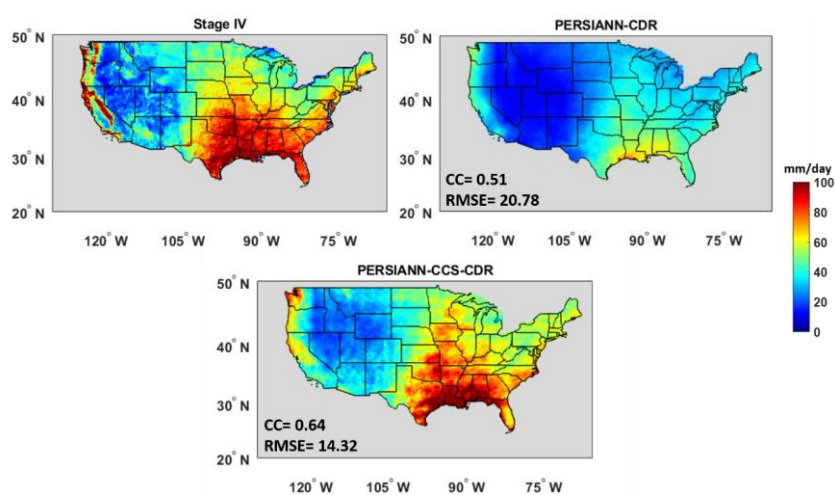
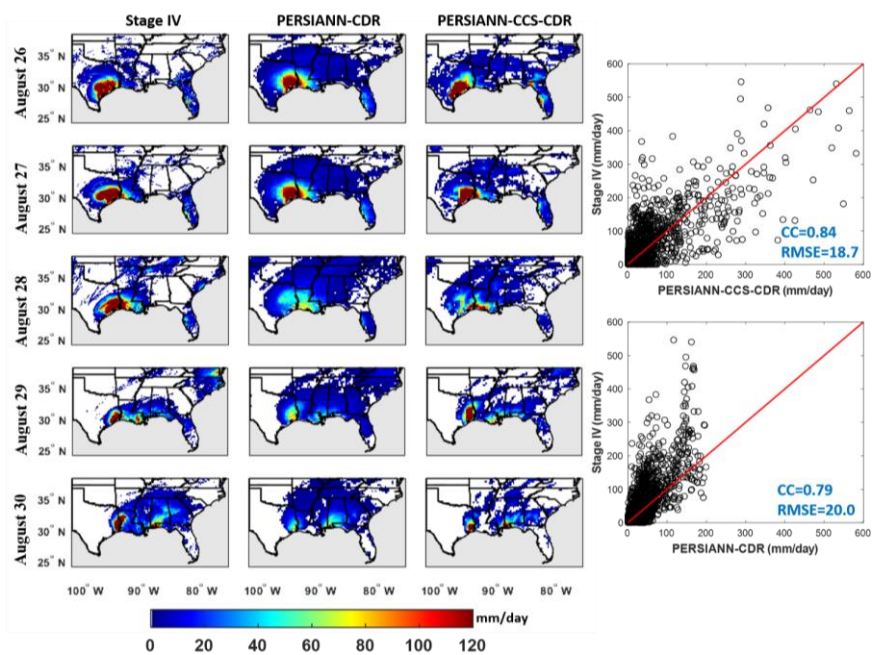


Figure 3



639

640

641

642

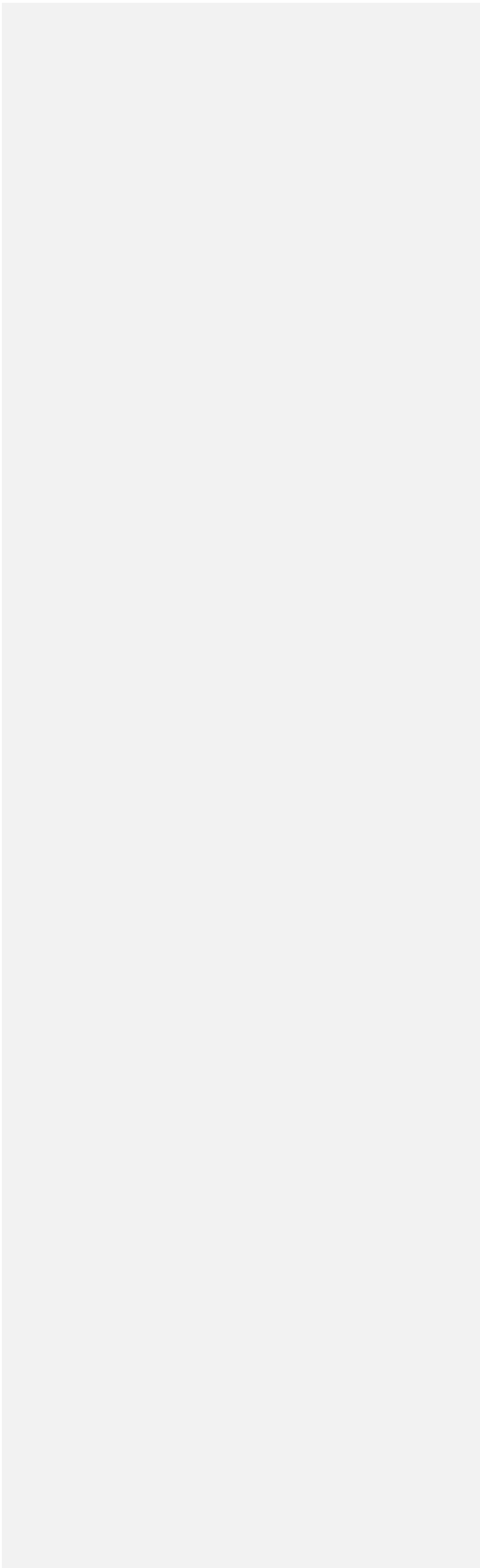
643

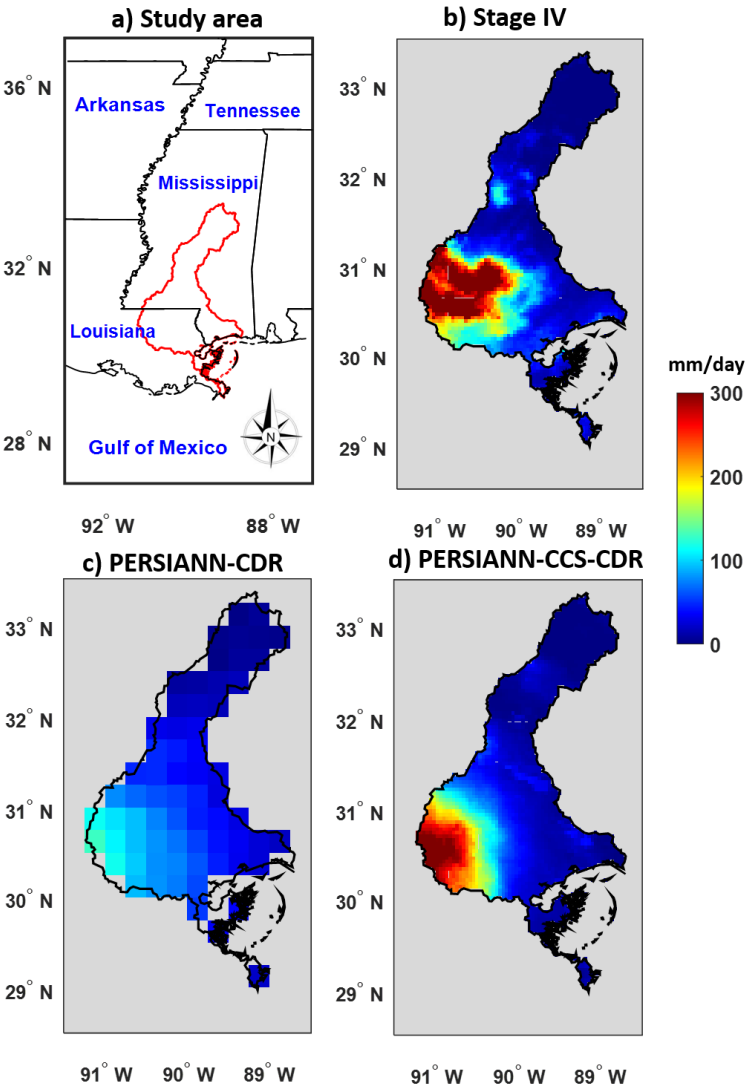
644

645

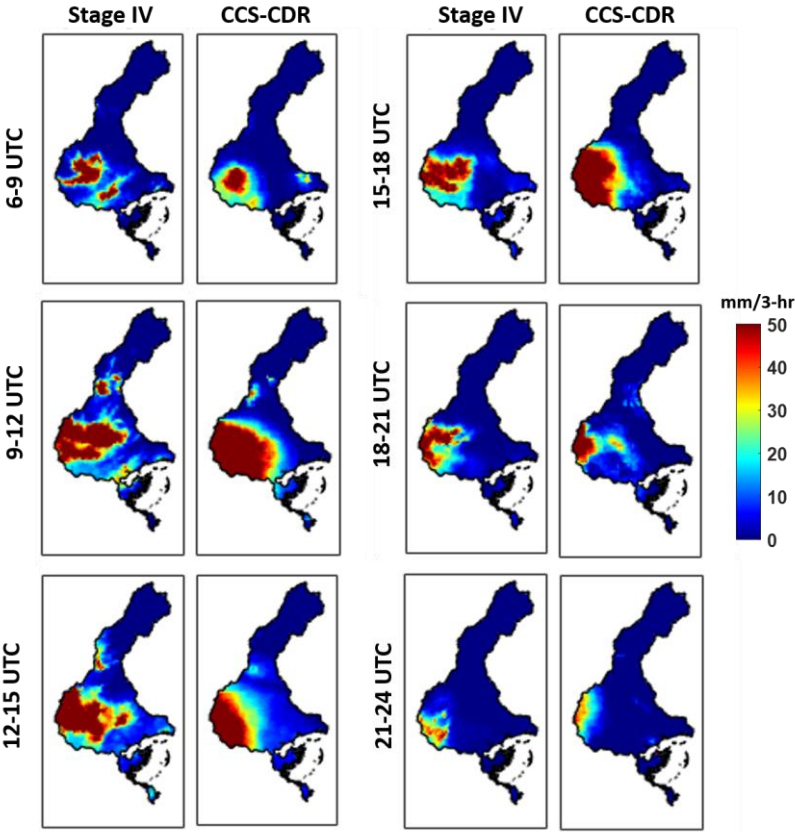
646

647 **Figure 4**





653



654

655

656

657

658

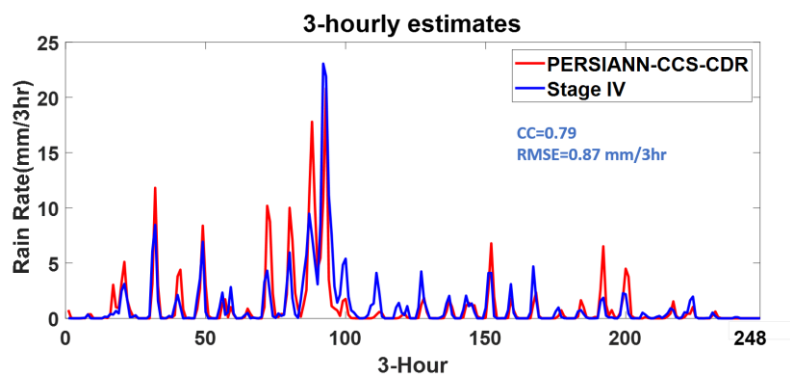
659

660

661

662

663 **Figure 6**



685 **Tables**

686 Table 1 An overview of available operational satellite-based precipitation estimation
687 products with their coverage and spatiotemporal resolutions.

688

689

690 Table 2 Summary of 3-hourly precipitation estimation performance of PERSIANN-CCS-
691 CDR for the Louisiana flood of Aug. 12, 2016 at $0.04^{\circ} \times 0.04^{\circ}$ spatial resolution.

692

693

694

695

696

697

698

699

700

701

702

703

704

705

706

707

708

709

710

711

712

713

714

715

716

717

718

719

Table 1

720
721

Product	Full name	Spatial resolution	Spatial coverage	Temporal resolution	Temporal coverage	Reference
CHIRPS	Climate Hazards group Infrared Precipitation with Stations	0.05°	50°S–50°N	Daily	1981-present	²⁰
CMAP	Climate Prediction Center (CPC) Merged Analysis of Precipitation	2.5°	90°S–90°N	Monthly/Pentad	1979-present	⁴⁴
CMORPH	CPC morphing technique	0.25°	60°S–60°N	Daily	1998-present	⁴⁵
GPCP	Global Precipitation Climatology Project (GPCP)	0.5°	90°S–90°N	Monthly/Pentad	1979-present	³¹
GPCP-1DD	Global Precipitation Climatology Project (GPCP) 1-Degree Daily (1DD) Combination	1°	90°S–90°N	Daily	1996-2015	⁴⁶
IMERG	Integrated Multi-satellite Retrievals for GPM	0.1°	60°S–60°N	30 min	2014-present	⁴⁷
MSWEP	Multi-Source Weighted-Ensemble Precipitation (MSWEP)	0.1°	90°S–90°N	3-hourly	1979-2017	^{48,49}
PERSIANN	Precipitation Estimation from Remotely Sensed Information using Artificial Neural Networks	0.25°	60°S–60°N	1-hourly	2000–present	⁵⁰
PERSIANN-CCS	PERSIANN-Cloud Classification System	0.04°	60°S–60°N	1-hourly	2003–present	⁵¹
PERSIANN-CDR	PERSIANN–Climate Data Record	0.25°	60°S–60°N	Daily	1983-present	¹²
PERSIANN-CCS-CDR	PERSIANN-Cloud Classification System-Climate Data Record	0.04°	60°S–60°N	3-hourly	1983-present	This paper
TMPA 3B42	TRMM Multi-satellite Precipitation Analysis	0.25°	50°S–50°N	3-hourly	1998-present	⁵²

722 **Table 2**
723
724

Criteria	PERSIANN-CCS-CDR
POD	0.85
FAR	0.24
CSI	0.67
RMSE (mm/3hr)	13.6
MAE (mm/3hr)	6.12
CC	0.64

725